Observation of Radar Echoes from High-Energy Particle Cascades

S. Prohira[,1,*] K. D. de Vries[,2] P. Allison,[1] J. Beatty[,1] D. Besson[,3,4] A. Connolly[,1] N. van Eijndhoven[,2]
C. Hast[,5] C.-Y. Kuo,[6] U. A. Latif[,3] T. Meures,[7] J. Nam,[6] A. Nozdrina[,3] J. P. Ralston,[3]
Z. Riesen[,8] C. Sbrocco,[1] J. Torres[,1] and S. Wissel[8]

[1]*Center for Cosmology and AstroParticle Physics (CCAPP), The Ohio State University, Columbus, Ohio 43210, USA*
[2]*Vrije Universiteit Brussel, Brussel 1050, Belgium*
[3]*University of Kansas, Lawrence, Kansas 66045, USA*
[4]*National Research Nuclear University, Moscow Engineering Physics Institute, Moscow 115409, Russia*
[5]*SLAC National Accelerator Laboratory, Menlo Park, California 94025, USA*
[6]*National Taiwan University, Taipei 10617, Taiwan*
[7]*University of Wisconsin-Madison, Madison, Wisconsin 53706, USA*
[8]*California Polytechnic State University, San Luis Obispo, California 93407, USA*

We report the observation of radar echoes from the ionization trails of high-energy particle cascades. Data were taken at the SLAC National Accelerator Laboratory, where the full electron beam ($\sim10^9$ e^- at ~10 GeV$/e^-$) was directed into a plastic target to simulate an ultrahigh-energy neutrino interaction. The target was interrogated with radio waves, and coherent radio reflections from the cascades were detected with properties consistent with theoretical expectations. This is the first definitive observation of radar echoes from high-energy particle cascades, which may lead to a viable neutrino detection technology for energies $\gtrsim 10^{16}$ eV.

Introduction.—Ultrahigh-energy (UHE) ($\gtrsim 10^{16}$ eV) astrophysical neutrinos offer great discovery potential. They would probe the accelerators of UHE cosmic rays, which are detected up to $\sim 10^{20}$ eV. Unlike cosmic rays, which are downscattered on the cosmic microwave background and also deflected in magnetic fields, detected neutrinos will point back to their sources. UHE neutrino-nucleon interactions probe center-of-mass energies above the energy scale of colliders, allowing sensitive tests of new physics. To fully exploit the scientific potential of UHE neutrinos, we ultimately need an observatory with sufficient exposure to collect high statistics even in pessimistic flux scenarios.

When UHE neutrinos interact in matter, they produce a relativistic cascade of particles, as well as a trail of nonrelativistic electrons and nuclei produced through the energy loss of the relativistic particles. The time-integrated cascade profile in ice is a ellipsoid of length ~10 m and radius ~0.1 m. Nearly all of the primary interaction energy goes into ionization of the medium.

The incoherent optical Cherenkov emission from individual cascade electrons and positrons can be detected in TeV–PeV detectors like IceCube [1] and similar experiments [2–4]. Yet due to the steeply falling neutrino spectrum, the optical detection rate of the proposed successor IceCube-Gen2 [5] is too small to make an adequate UHE observatory. Several more efficient technologies have been proposed and implemented to detect

cascades from UHE neutrinos. First, the coherent radio frequency (rf) emission from a net charge asymmetry in the cascade (the Askaryan effect [6]) has been observed in the laboratory [7] and is the focus of a variety of past [8], present [9–11], and proposed [12,13] experiments. Radio methods (detailed in Refs. [14,15]) can instrument large volumes more sparsely than optical detectors due to the transparency of radio in ice [16–20], making the construction of a large detector more cost-effective. Second, a τ neutrino, interacting in Earth, can produce a τ lepton—carrying much of the primary ν_τ energy—that exits Earth and decays in air, producing a cascade. A current is induced in this cascade as it moves relativistically through Earth's geomagnetic field, leading to coherent radio emission [21–25] that might be detected by proposed experiments [26–28]. Third, the fluorescence and Cherenkov light from such in-air decays can be detected by balloon-or satellite-borne experiments [29–31]. These methods have potential for discovery at very high energies. However, they have limited sensitivity at the lower end of the UHE range, from 10^{16} to 10^{17} eV (10–100 PeV), just above the reach of optical Cherenkov detectors like IceCube.

Finally, it has been proposed that cascades can be detected by radar reflections off their ionization trail. This technique shows promising projected sensitivity down to $\sim$ PeV energies [32,33] and—coupled with the steeply falling neutrino flux—is currently the only technique forecasted to have peak sensitivity in the 10–100 PeV

range. This creates the potential to close the gap between optical Cherenkov detectors and the high-energy technologies listed above. To that end, several recent experimental efforts [34–36] have made incremental progress toward the detection of a radar echo from a cascade in a dense medium.

In this Letter, we present the first definitive observation of a radar echo from a particle cascade. This observation was made by experiment T576 at the SLAC National Accelerator Laboratory, where their electron beam ($\sim 10^9$ e^- at $\sim 10^{10}$ eV/e^-) was used to produce a particle cascade with a density equivalent to that of a $\sim 10^{19}$ eV neutrino interaction in ice and with a similar shower profile. A transmitting antenna (TX) broadcast continuous-wave (CW) radio toward the cascade and several receiving antennas (RX) monitored for a radar reflection. We report on the observation of a signal consistent with theoretical predictions. Below, we detail the experiment, analysis technique, and results.

Experimental setup and data collection.—The experiment, depicted in Fig. 1, took place at End Station A at SLAC. Designated T576, the experiment had two runs during 2018, one in May after which a suggestion of a reflection was reported [37], and a second run in October, which is the focus of the present Letter. We broadcast CW radio at a range of frequencies between 1 and 2.1 GHz and a range of amplitudes, using a signal generator, 50 W power amplifier, and transmitting antenna toward a target of high-density polyethylene (HDPE, borrowed from the
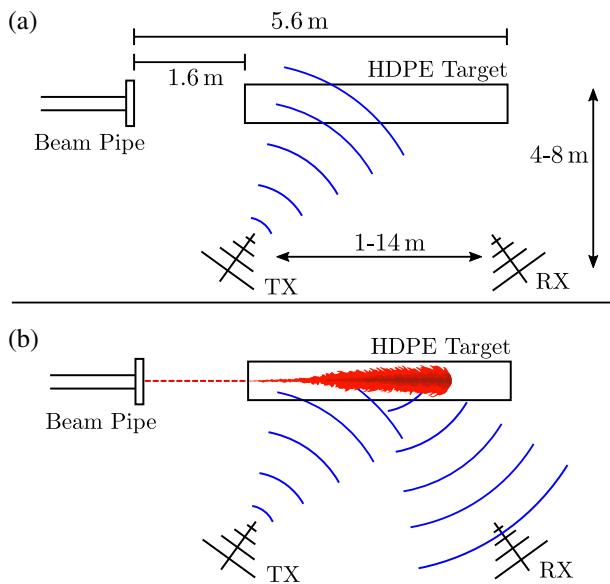

FIG. 1. Cartoon of the radar method and T576, with range of experimental dimensions indicated (antennas were placed in various configurations). (a) A transmitter (TX) illuminates a target. (b) The beam exits the beam pipe and creates a cascade inside the target, leaving behind an ionization cloud. The transmitted signal is reflected to a monitoring receiver (RX). Not to scale.

T510 experiment [38]), into which the electron beam was directed. Receiving antennas were also directed at this target to measure the radar reflection. The data presented in this Letter were captured by a Tektronix 4 channel, 20 GS/s oscilloscope.

Two different types of antennas were used in this analysis. One was a Vivaldi-style, ultrawideband antenna (0.6–6 GHz) with a measured forward gain of +12 dBi at 2 GHz, and the other was a custom-built 0.9–4 GHz log-periodic dipole antenna (LPDA). The LPDA was used in conjunction with a parabolic dish reflector, with a measured forward gain of +18 dBi at 2 GHz. Surrounding the beam pipe exit was an integrating current toroid (ICT), which gave a precise measurement of the charge in each bunch, and provided a very stable reference point for post-run alignment of the dataset.

The data taking was separated into sub-runs consisting of 100–500 events. Between sub-runs, certain parameters (TX frequency, TX amplitude, TX position, and RX position) were varied. Runs in which data were taken for analysis are called signal runs. Other sub-runs were reserved for taking background data and are called background runs. The experiment lasted 8 days, with over 4 full days of beam time acquired in 12-hour increments.

The three main improvements over the first run of T576 were (i) the use of a power amplifier capable of reaching higher frequencies, to overcome the primary rf backgrounds (discussed below) that are dominant at frequencies $\lesssim 1$ GHz, (ii) higher gain antennas, and (iii) a faster oscilloscope (20 GS/s) for greater precision in the time domain waveforms.

Expectations.—The radar method had been suggested for cosmic-ray initiated extensive-air-shower (EAS) detection in the atmosphere as early as 1940 [39,40], with further development in the 1960s [41], followed by stagnation, and then renewed interest in the early 2000s [42–44]. Recent experimental searches from terrestrial radar systems [45] and a dedicated experiment, Telescope Array RAdar (TARA) [46,47], reported no signal due to collisional losses—which limit the efficiency of the scattering—and insufficient ionization density in air. Short free-electron lifetimes ($\tau \sim$ ns) in air at EAS altitudes cause the ionization to vanish before a sufficient density to reflect incident rf can be achieved. Cascades in ice or other dense media do not suffer from this problem.

The theory for radar is well established, and models of radar detection of cascades in dense media have evolved to maturity in recent years. Whether built up from a macroscopic [32] or first-principles [33] viewpoint, the properties of a reflection are well defined and subject to several properties of the material in which the cascade happens. The density of the ionization is strongly dependent upon the density of the medium. Another critical parameter is the mean ionization lifetime of the material. This lifetime τ dictates the longitudinal extent of the ionization deposit,

and thus the overall length scale of the reflector. For ice, τ ranges from $\mathcal{O}[1 \text{ to } 10]$ ns and is strongly dependent upon the temperature of the ice [48]. For HDPE, the lifetimes are comparable to those of cold polar ice [49].

For a given transmitter and receiver, the spectral content of the reflected signal is a function of τ and the cascade geometry. For a compact cascade, as was the case for T576, any lifetime exceeding 1 ns would produce a significant radar reflection at the transmitted frequency. In nature, a UHE cascade of similar density would be longer by a factor of ~few in ice, which is expected to cause an effective Doppler shift depending upon the radar geometry. We transmitted at a peak power of 50 W, with no amplification on our receivers. The expected signal for T576 was a radar return of a few ns in duration, at the transmitter frequency, at a level of a few mV.

Data analysis.—The data analysis for T576 was challenging because of the high-amplitude backgrounds. When a charge bunch such as the SLAC beam traverses media with differing indices of refraction, or effective indices of refraction, transition radiation of various forms [50–52] is produced. These signals—which would not be present in nature [53]—exceeded our expected radar signal by a factor of 10–100 in amplitude. Fortunately, the total rf background caused by the beam (called "beam splash") was quite stable. This background was characterized and filtered using a sensitive matrix-decomposition technique, detailed in Ref. [54] and based on Ref. [55], that we call singular-value-decomposition (SVD) filtration.

There are four nominal components to the signal run data: CW, beam splash, noise, and signal (a radar reflection). The background run data contain only beam splash and noise. Since the response of our system is linear for the range of signals received, the total background to our signal is a linear combination of CW, beam splash, and thermal noise. We call this linear combination "null data." To build the null data, we added presignal-region CW from signal run data to signal-region beam splash in background run data.

SVD filtration identifies and removes patterns, features in the data that are found in multiple individual measurements, such as the beam splash and CW. The SVD filtration characterizes these patterns within a set of carefully aligned null data, producing a filter basis. Then a filter is produced for each individual event by expanding it in the filter basis. After applying this filter, the only thing remaining in the event should be random, featureless background noise, and any putative signal present in the real data.

The filtration process was a blind procedure, tuned on a number of sub-runs comprising $< 10\%$ of the data. In addition, a null event was constructed for every real event in the full dataset to serve as the null hypothesis. An SVD filter was constructed for each signal run according to its associated background run, and both datasets (real and null) were filtered using the same SVD-filter basis. The resultant filtered data was then analyzed for excess.
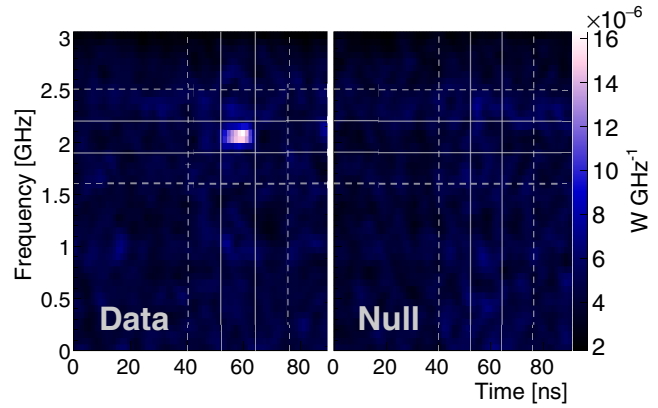

FIG. 2. Left: time-versus-frequency (spectrogram) representation of the observed signal in data. This is the average of 200 events in a single signal run. Right: the same representation for the associated null data set for this sub-run. In both plots, the cross-hairs indicate the signal and sideband regions used to calculate the significance as described in the main text.

Results.—To investigate both the time and spectral content of the signal, a time-versus-frequency spectrogram was generated for each filtered event in a signal run, and these spectrograms were averaged. The result of such a process is shown in Fig. 2, where a clear excess is visible in the real data—and not in the null data—at the transmitter frequency of 2.1 GHz with a duration of a few ns. A similar excess was observed at various transmit frequencies, antenna positions, and in different antennas. No excess is observed at the same time and frequency point in the null data. Signal and sideband regions are indicated by the solid and dashed lines, respectively.

The highest amplitude signal was expected and received during runs with a horizontally polarized, high-gain antenna at the specular angle, where the resultant (SVD filtered) signal was large enough to extract a time-domain waveform through careful timing alignment and averaging. Events were aligned so that none could shift by more than a fraction of a transmit period and then averaged. A resultant time-domain average is shown in Fig. 3, where only events that had high enough SNR for reliable cross-correlation are used in order to facilitate *qualitative* comparison to simulation. Also, in Fig. 3 is a comparison to a finite difference time domain (FDTD) simulation of the same signal run (including CAD models of the actual antennas used and the same target material, with a time-dependent conducting volume modeled using a GEANT4 [56] simulation of the SLAC beam). There is also a comparison to the RadioScatter particle-level simulation code [57], which runs within GEANT4 driven by a model of the SLAC beam. The simulations have been scaled (-20% for FDTD, -35% for RadioScatter) to allow comparison of the waveform shapes and aligned in time with the data. Systematic uncertainties on the true signal amplitude are presented in Table I. The plasma lifetime—the main free parameter in both simulations—is set to $\tau = 3$ ns.
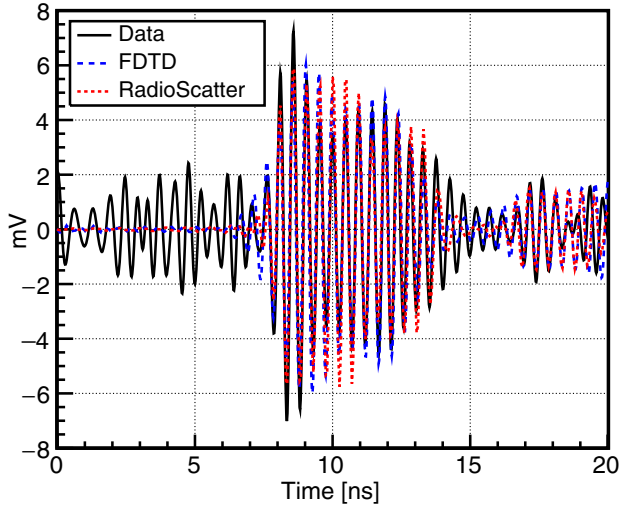
FIG. 3.   An example time-domain average of the highest-SNR reflections from a signal run (solid black), compared to the output of an FDTD simulation for the same signal run (dashed blue), and a RadioScatter simulation for the same signal run (dashed red). The plasma lifetime for the simulation is 3 ns.

Several checks were performed to establish that the observed signal has properties consistent with a radar echo. To demonstrate that the signal was observed consistently in multiple antenna or frequency or power configurations, in Fig. 4 we show the effective scattering cross section, σ_{eff}, as a function of transmitter power. This expression (discussed in Ref. [33]) is a measure of the effective "size" of the reflecting region, should have a weak dependence on frequency at these energies, and should be constant with transmitted power ($\sigma_{\mathrm{eff}} \propto P_{\mathrm{rec}}/P_{\mathrm{tran}}$). All of these attributes are observed for the signal, which is shown in comparison to RadioScatter simulation (solid bands, including systematic error of HDPE collisional frequency, which is ionization energy dependent [58]). The errors in the measurement of σ_{eff} include statistical and systematic uncertainties (tabulated in Table I along with the dependence of each error). Some errors affect the overall level of all received signal amplitudes (globally dependent) while others would introduce systematic offsets between antennas (antenna-to-antenna dependent). Trending of the signal with antenna baselines was not observed, owing to the fact that our antennas were not in the diffractive far field. This nonobservation of such trends was verified by FDTD simulations.

Because the signal is so small relative to the beam splash, and the null hypothesis relies on a linear combination of background components, an obvious concern is a nonlinearity in the overall system. After the run, a series of tests were performed in which CW at the same frequency and amplitude as T576 was amplified and broadcast via a Vivaldi antenna, and another Vivaldi, connected to an oscilloscope, was set up as a receiver. A high-voltage pulse with similar spectral content and

TABLE I.   Sources of systematic error (in dB of received power), and their associated estimated errors, used in Fig. 4. Indicated in the right column is the dependence of the individual systematic on the data, either antenna-to-antenna dependent (A), frequency dependent (F), power dependent (P), or globally dependent (G).

Systematic	Estimated error (dB)	Dependence
Room effects	3	A,F,G
Antenna gain/orientation	1	A,F
Cable loss measurement	1	P
TX output power	2	P,G

amplitude ($\mathcal{O}[100~\mathrm{mV}]$) to the beam splash was broadcast simultaneously. The same analysis technique explained here, involving construction of null data and SVD filtration, was performed on these data, and no excess was observed.

To establish a significance against a random fluctuation of the background, we generated $N = 10^7$ sets of 100 null events via bootstrapping, made an average spectrogram (like in Fig. 2) for each set, and evaluated a test statistic of the sideband-subtracted power excess in the signal region. The signal region, tuned on a discarded subset of the data, is outlined in Fig. 2. The value of the test statistic (μW ns) in the null data is $\mathrm{TS_{null}} = 2.20^{+6.56}_{-6.20}$. The value of the test statistic in the measured data is $\mathrm{TS_{data}} = 61.2^{+7.40}_{-6.58}$, well in excess of the 5σ quantile.
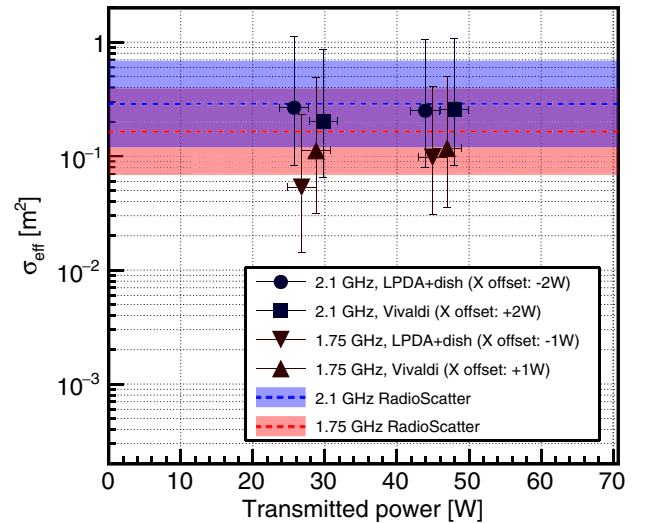

FIG. 4.   The effective scattering cross section, σ_{eff}, as a function of transmitter output power, for various receiving antennas (LPDA + dish and Vivaldi) and two different frequencies. Errors are statistical and systematic, and dominated by the latter. Each set of four points has been clustered around the true X-axis value, for clarity, with the offset indicated in the figure legend. The solid bands are σ_{eff} from RadioScatter, including statistical and systematic errors.

Discussion and conclusions.—We have reported the observation of radar reflections from a particle-shower induced cascade in a dense material. We have shown that the signal is in good agreement with theoretical expectations and has a negligible probability of being a background fluctuation. This detection has promising implications for UHE neutrino detection, particularly in the 10–100 PeV range.

Experiment T576 provided a good replica for an in-ice neutrino interaction with respect to the cascade density, the ionization lifetime, and the radio properties of the medium. In nature, a single high-energy primary—as opposed to the large number of lower energy primaries at SLAC—would result in a longer radar echo by a factor of a few, aiding in direction and energy reconstruction of individual events.

---

*prohira.1@osu.edu

[1] M. G. Aartsen *et al.* (IceCube Collaboration), Science **342,** 1242856 (2013).

[2] M. Ageron *et al.* (ANTARES Collaboration), Nucl. Instrum. Methods Phys. Res., Sect. A **656,** 11 (2011).

[3] A. D. Avrorin *et al.* (BAIKAL Collaboration), Nucl. Instrum. Methods Phys. Res., Sect. A **742,** 82 (2014).

[4] A. Margiotta (KM3NeT Collaboration), Nucl. Instrum. Methods Phys. Res., Sect. A **766,** 83 (2014).

[5] J. van Santen (IceCube Gen2 Collaboration), Proc. Sci., ICRC2017 (**2018**) 991.

[6] G. A. Askar'yan, Zh. Eksp. Teor. Fiz. **41,** 616 (1961) [Sov. Phys. JETP **14,** 441 (1962)].

[7] D. Saltzberg, P. Gorham, D. Walz, C. Field, R. Iverson, A. Odian, G. Resch, P. Schoessow, and D. Williams, Phys. Rev. Lett. **86,** 2802 (2001).

[8] I. Kravchenko *et al.*, Phys. Rev. D **73,** 082002 (2006).

[9] P. Allison *et al.*, Astropart. Phys. **35,** 457 (2012).

[10] P. W. Gorham *et al.* (ANITA Collaboration), Astropart. Phys. **32,** 10 (2009).

[11] S. Klein *et al.*, IEEE Trans. Nucl. Sci. **60,** 637 (2013).

[12] C. Deaconu (ANITA Collaboration), Proc. Sci., ICRC2019 (**2019**) 867.

[13] J. A. Aguilar *et al.*, arXiv:1907.12526.

[14] F. G. Schröder, Prog. Part. Nucl. Phys. **93,** 1 (2017).

[15] T. Huege and D. Besson, Prog. Theor. Exp. Phys. **2017,** 12A106 (2017).

[16] E. Zas, F. Halzen, and T. Stanev, Phys. Rev. D **45,** 362 (1992).

[17] G. M. Frichter, J. P. Ralston, and D. W. McKay, Phys. Rev. D **53,** 1684 (1996).

[18] S. Barwick, D. Besson, P. Gorham, and D. Saltzberg, J. Glaciol. **51,** 231 (2005).

[19] J. Avva, J. M. Kovac, C. Miki, D. Saltzberg, and A. G. Vieregg, J. Glaciol. **61,** 1005 (2015).

[20] D. Besson, J. Jenkins, S. Matsuno, J. Nam, M. Smith, S. Barwick, J. Beatty, W. Binns, C. Chen, P. Chen *et al.*, Astropart. Phys. **29,** 130 (2008).

[21] F. D. Kahn and I. Lerche, Proc. R. Soc. A **289,** 206 (1966).

[22] O. Scholten, K. Werner, and F. Rusydi, Astropart. Phys. **29,** 94 (2008).

[23] H. Falcke, W. Apel, A. Badea, L. Bähren, K. Bekk, A. Bercuci, M. Bertaina, P. Biermann, J. Blümer, H. Bozdog *et al.*, Nature (London) **435,** 313 (2005).

[24] D. Ardouin, A. Belletoile, D. Charrier, R. Dallier, L. Denis, P. Eschstruth, T. Gousset, F. Haddad, J. Lamblin, P. Lautridou *et al.*, Astropart. Phys. **26,** 341 (2006).

[25] A. Aab, P. Abreu, M. Aglietta, M. Ahlers, E. Ahn, I. Albuquerque, I. Allekotte, J. Allen, P. Allison, A. Almela *et al.*, Phys. Rev. D **89,** 052002 (2014).

[26] J. Alvarez-Muñiz *et al.* (GRAND Collaboration), Sci. China Phys. Mech. Astron. **63,** 219501 (2020).

[27] S. Wissel, J. Alvarez-Muniz, C. Burch, A. Cummings, W. Carvalho, C. Deaconu, G. Hallinan, K. Hughes, A. Ludwig, E. Oberla, C. Paciaroni, A. Rodriguez, A. Romero-Wolf, H. Schoorlemmer, D. Southall, B. Strutt, M. Vasquez, A. Vieregg, and E. Zas, Proc. Sci., ICRC2019 (**2019**) 1033.

[28] J. Nam, P. Chen, Y. Chen, S. Hsu, J. Huang, M. Huang, C. Kuo, C. Leung, T. Liu, B. Shin, Y. Shiao, M. Wang, S. Wang, C. Hornhuber, and A. Novikov, Proc. Sci. ICRC2019 (**2019**) 967.

[29] J. H. Adams *et al.*, arXiv:1703.04513.

[30] J. H. Adams *et al.* (JEM-EUSO Collaboration), Astropart. Phys. **44,** 76 (2013).

[31] A. V. Olinto *et al.*, Proc. Sci., ICRC2017 (**2018**) 542.

[32] K. D. de Vries, K. Hanson, and T. Meures, Astropart. Phys. **60,** 25 (2015).

[33] S. Prohira and D. Besson, Nucl. Instrum. Methods Phys. Res., Sect. A **922,** 161 (2019).

[34] M. Chiba *et al.*, arXiv:0710.4186v1.

[35] M. Chiba *et al.*, AIP Conf. Proc. **1535,** 45 (2013).

[36] K. DeVries *et al.*, Proc. Sci., ICRC2017 (**2017**) 1049.

[37] S. Prohira *et al.*, Phys. Rev. D **100**, 072003 (2019).

[38] K. Belov *et al.* (T-510 Collaboration), Phys. Rev. Lett. **116**, 141103 (2016).

[39] P. Blackett and C. Lovell, Proc. R. Soc. A **177**, 183 (1941).

[40] A. C. B. Lovell, Notes Rec. R. Soc. **47**, 119 (1993).

[41] T. Matano, M. Nagano, K. Suga, and G. Tanahashi, Can. J. Phys. **46**, S255 (1968).

[42] P. Gorham, Astropart. Phys. **15**, 177 (2001).

[43] J. Stasielak, R. Engel, S. Baur, P. Neunteufel, R. Šmída, F. Werner, and H. Wilczyński, Astropart. Phys. **73**, 14 (2016).

[44] M. I. Bakunov, A. V. Maslov, A. L. Novokovskaya, and A. Kryemadhi, Astropart. Phys. **33**, 335 (2010).

[45] T. Terasawa, T. Nakamura, H. Sagawa, H. Miyamoto, H. Yoshida, and M. Fukushima, in *Proceedings of the 31st International Cosmic ray Conference* (2009).

[46] R. Abbasi *et al.*, Nucl. Instrum. Methods Phys. Res., Sect. A **767**, 322 (2014).

[47] R. U. Abbasi *et al.*, Astropart. Phys. **87**, 1 (2017).

[48] M. P. De Haas, M. Kunst, J. M. Warman, and J. B. Verberne, J. Phys. Chem. **87**, 4089 (1983).

[49] R. Weingart, R. Barlett, R. Lee, and W. Hofer, IEEE Trans. Nucl. Sci. **19**, 15 (1972).

[50] V. L. Ginzburg and I. M. Frank, Zh. Eksp. Teor. Fiz. **16**, 15 (1946) [J. Phys. (USSR) **9**, 353 (1945)].

[51] K. D. de Vries *et al.*, Phys. Rev. D **98**, 123020 (2018).

[52] P. W. Gorham, D. P. Saltzberg, P. Schoessow, W. Gai, J. G. Power, R. Konecny, and M. E. Conde, Phys. Rev. E **62**, 8590 (2000).

[53] Except for the case of a cascade crossing the air/ice boundary, either an in-ice neutrino cascade breaking out into the air, or an in-air cosmic ray cascade breaking into the ice. Sensitivity to such events is subject to the orientation of transmit and receive antennas and will be explored.

[54] S. Prohira (T576 Collaboration), arXiv:1910.11314.

[55] A. Bean, J. P. Ralston, and J. Snow, Nucl. Instrum. Methods Phys. Res., Sect. A **596**, 172 (2008).

[56] S. Agostineli *et al.*, Nucl. Instrum. Methods Phys. Res., Sect. A **506**, 250 (2003).

[57] S. Prohira, https://github.com/prchyr/RadioScatter (2017).

[58] Y.-K. Kim, K. Irikura, M. Rudd, M. Ali, P. Stone, J. Chang, J. Coursey, R. Dragoset, A. Kishore, K. Olsen, A. Sansonetti, G. Wiersma, D. Zucker, and M. Zucker, Electron-impact ionization cross section for ionization and excitation database (version 3.0) (2004), https://doi.org/10.18434/T4KK5C.